

A Stable Vision-Based Control Scheme for Nonholonomic Vehicles to Keep a Landmark in the Field of View

Nicholas R. Gans¹ and Seth A. Hutchinson²

Abstract—Control of wheeled vehicles is a difficult problem due to nonholonomic constraints. This problem is compounded by sensor limitations. A previously developed control scheme for a wheeled robot, which keeps a target in the view of a mounted camera, is one solution to the problem. In this paper, we prove the controllability and stability of the control scheme. We present an implementation of the controller, as well as present the results of simulations and physical experiments.

I. INTRODUCTION

Many mobile robots fall into the category of nonholonomic vehicles, which are typically underactuated and have constraints on derivatives of the configuration variables. Typical feedback control methods offer poor results or may not work at all.

The field of nonholonomic motion planning has grown to address these issues [1]. Path planning is difficult under the best of circumstances, and becomes more difficult when limitations of sensors are taken into account. In this paper we focus on the situation of a kinematic unicycle vehicle with an on board camera as the only sensor.

Since the velocities available to a nonholonomic system are limited, one popular solution is to use piecewise continuous control to move in a series of steps. Keeping a landmark in the field of view effectively constrains direction and size of these steps.

Pissard-Gibollet and Rives [2] detailed the problems of using vision-based control with nonholonomic vehicles and overcome these problems by adding additional degrees of freedom to the camera. Ma et al. [3] established vision-based feedback control of a unicycle and car-like robots using advanced techniques in nonholonomic path planning. Fang et al. [4] controlled a mobile robot using Position Based Visual Servoing techniques based on planar homography. Kantor and Rizzi [5] independently designed a vision-based controller that produces oscillating velocities to follow very similar trajectories to those presented here using .

Bhattacharya et al. [6] developed a control scheme to provide a continuous, piecewise smooth trajectory to a unicycle robot while keeping a landmark in the field of view. That paper focused on proving the least distance optimality of the control scheme. This paper proves controllability and stability of the scheme, i.e. the robot can be regulated to any point in the task space. Furthermore, this paper details the use

of the control scheme with a real robot system. The scheme in [6] required 3D information such as depth to the landmark. In an effort to make this an entirely vision-based algorithm (for instance no distance sensors are used), some adaptations are made to the algorithm. In light of these adaptations, it can be claimed that the implementation approximates the controller. Nevertheless, simulated and experimental results are very promising.

In Section II we provide background information on the kinematic unicycle and the method developed by [6]. In Section III we offer a proof of controllability, and in Section IV we give a proof of asymptotic regulation to a goal pose. In Section V we detail a implementation of the controller using a camera as the only sensor, and simple feedback control laws. Finally, in Section VI we provide results of simulations using the newly introduced vision-based controller.

II. BACKGROUND

A. Keeping a landmark in the field of view.

Bhattacharya et al. introduced a novel scheme to move a kinematic unicycle while keeping a landmark within the field of view of a camera mounted on the robot [6]. This paper primarily focused on the properties of the paths generated by the scheme, especially optimality of path length. We will focus on a vision-based implementation of this control scheme and properties of reachability and stability.

Consider a mobile robot in the plane. A landmark consisting of a point is located at the origin. At time $t = 0$ the robot lies within an annulus centered at the origin and defined by a minimum and maximum radii, r_{\min} and r_{\max} , respectively. For simplicity, assume the camera is mounted such that the optical center is above the origin of the robot body reference frame, and the optical axis is parallel to the robot x axis. The angle ϕ measures the angle from the optical axis to the line from the origin of the world frame to origin of the body frame. This is seen in Fig. 1.

To keep a landmark at the origin within the field of view, the robot must be pointed toward the landmark. This adds a constraint

$$\psi + \phi = \pi + \tan^{-1} \frac{y}{x} = \pi + \theta. \quad (1)$$

The maximum viewable angle on the right side of the camera is defined as $\tilde{\phi}$, as measured from the robot x -axis, and maximum viewable angle on the left as $\tilde{\phi}$. If $\phi \in [-\tilde{\phi}, \tilde{\phi}]$ then a point at the origin is visible in the image. Again, this can be seen in Fig. 1.

The control scheme in [6] features two modes of operation. Rotating the robot until the image of the landmark (in this

¹N. Gans is with the Department of Mechanical and Aerospace Engineering, University of Florida, Gainesville, FL USA, ngans@ufl.edu

²S. Hutchinson is with the Department of Electrical and Computer Engineering, University of Illinois at Urbana-Champaign, Urbana, IL USA, seth@uiuc.edu

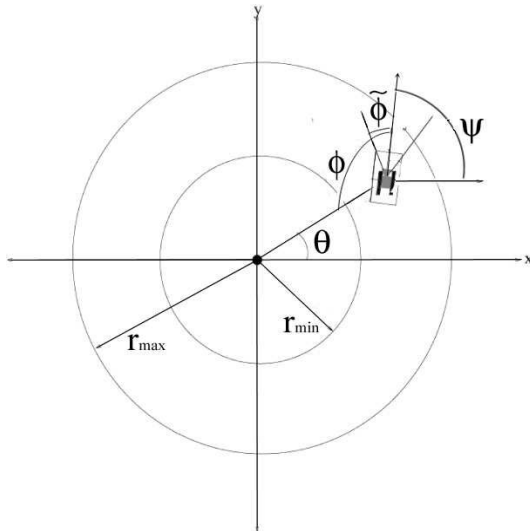


Fig. 1. Coordinate assignments for a kinematic unicycle robot with camera

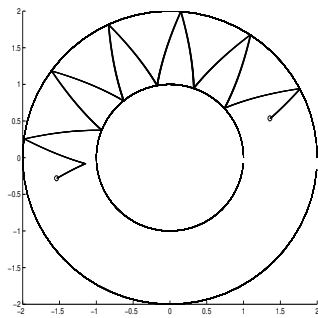


Fig. 2. An S-curve for $\phi = \frac{\pi}{6}$

case, a single point at the origin) was on the edge of the image ($\phi = \pm\tilde{\phi}$), and driving the robot forward or backward while keeping the image point on the edge of the image. This gives rise to a curved path, which was labeled a *T-curve*. From any point there are two available T-curves depending on if $\phi = \pm\tilde{\phi}$ and the robot can drive forward or backwards upon either. The T-curve through a point $[r_0, \theta_0]^T$ is described by the equation [6]

$$r = r_0 \exp \left\{ \frac{(\theta_0 - \theta)}{\tan \phi} \right\}. \quad (2)$$

By introducing the maximum and minimum value for the radius r , and alternating between the available T-curves each time the robot reaches r_{\min} and r_{\max} , it is possible to move about an annulus centered on the landmark. This collection of T-curves was named an *S-curve*, and is illustrated in figure II-A. As will be shown in Section III, an S-curve is available to move between any two points in the annulus while maintaining the landmark in the field of view.

B. The Kinematic Unicycle

We adopt the familiar kinematic unicycle model [1] for our nonholonomic vehicle. The local coordinates of the unicycle are $[x, y, \psi]^T$, where x and y are the position of the robot in plane and ψ is the angle from the world x -axis and robot

x -axis. This is illustrated in Fig. 1. The equations of state can be written in matrix form as

$$\begin{bmatrix} \dot{x} \\ \dot{y} \\ \dot{\psi} \end{bmatrix} = \begin{bmatrix} \cos \psi \\ \sin \psi \\ 0 \end{bmatrix} v + \begin{bmatrix} 0 \\ 0 \\ 1 \end{bmatrix} \omega \quad (3)$$

where v and ω are linear and angular velocity, respectively, and are inputs to the system.

It will ease future calculation to use polar coordinates in place of Cartesian coordinates. Under this change of coordinates, the system can be described by

$$\begin{bmatrix} \dot{r} \\ \dot{\theta} \\ \dot{\psi} \end{bmatrix} = \begin{bmatrix} \cos(\theta - \psi) \\ \frac{1}{r} \sin(\theta - \psi) \\ 0 \end{bmatrix} v + \begin{bmatrix} 0 \\ 0 \\ 1 \end{bmatrix} \omega.$$

III. PROOF OF CONTROLLABILITY

In this section, we will prove that the kinematic unicycle is controllable when constrained to drive along S-curves. It is known that a driftless system is small-time controllable if and only if the vector space spanned by the family of vector fields available to the system, along with their Lie brackets, is of full rank everywhere. This is also known as the Lie Algebra Rank Condition (LARC) or Chow's Theorem [7], [1], [8]. It can be shown that the kinematic unicycle is small-time controllable given the equation of motion (3)[1]. We now explore the case when the kinematic unicycle is constrained to the available T-curves.

The two T-curves available at each point provide two vector fields, f_1 and f_2 . Combining equations (4) and (1) gives

$$\cos(\theta - \psi) = -\cos(\phi) \quad (4)$$

$$\sin(\psi - \theta) = \sin(\phi). \quad (5)$$

Keeping the landmark at the edge of the image sets $\phi \in \{-\tilde{\phi}, \tilde{\phi}\}$. Taking the derivative of (1) along a T-curve then yields

$$\dot{\psi} = \dot{\theta}. \quad (6)$$

Equations (4),(5) and (6) are used to define the two vector fields

$$f_1 = \left[-\cos(\tilde{\phi})v, \frac{1}{r} \sin(\tilde{\phi})v, \frac{1}{r} \sin(\tilde{\phi})v \right]^T \quad (7)$$

$$f_2 = \left[-\cos(-\tilde{\phi})v, \frac{1}{r} \sin(-\tilde{\phi})v, \frac{1}{r} \sin(-\tilde{\phi})v \right]^T. \quad (8)$$

These two vector fields describe the velocities available by following T-curves.

We add a third vector field described by equation (3)

$$f_3 = [0, 0, \omega]^T. \quad (9)$$

Vector field f_3 rotates the robot to obtain a desired value of ψ .

We consider the admissible configuration space to be the collection of points satisfying $\{r, \theta, \psi | r \in [r_{\min}, r_{\max}], \theta \in (-\pi, \pi], \psi \in \mathbb{S}^1\}$, which can be viewed as a manifold with boundary and an embedded submanifold of $\mathbb{R}^2 \times SO(2)$. The configuration space is the Cartesian product of an

annulus and $SO(2)$, and we will refer to this space as $\mathcal{A} \subset \mathbb{R}^2 \times SO(2)$. In an abuse of terminology, we will refer to a state $\mathbf{X} = [r, \theta, \psi]^T \in \mathcal{A}$ as being *in the annulus* if $r \in [r_{\min}, r_{\max}]$.

The span of the vector fields $\{f_1, f_2\}$ loses rank when $\tilde{\phi} = n\pi/2$ for $n \in \mathbb{Z}$. A typical video camera has a cone of view much less than 90° , so the family will not lose rank due to this condition (we do not consider the case of fish eye lenses or catadioptric cameras, and in any event they are not subject to the same problems of field of view). Due to the mapping from Cartesian to polar coordinates, the fields f_1, f_2 experience a singularity at $r = 0$. However, since the annulus has a minimum radius r_{\min} bounded away from zero, so this too can be discounted.

Thus, using the span of the vector fields $\{f_1, f_2, f_3\}$ is full rank, and satisfies the LARC for all points in \mathcal{A} . Therefore the system using T-curves is small time controllable from any point in \mathcal{A} . For any goal value of the bearing ψ such that $\phi \notin [-\tilde{\phi}, \tilde{\phi}]$, (1) (i.e. the landmark is not visible for the goal ψ), the robot can be brought to the desired values of r and θ , then rotated to the desired orientation. However if the landmark leaves the field of view, feedback control cannot be used and final angular error is likely.

IV. STABILITY ANALYSIS

In this section we prove that a controller which drives a system along a series of T-curves is bounded and able to regulate the position of a vehicle to a goal pose from anywhere in the annulus. To this end we show that the error in the position variable θ is strictly decreasing and the system will reach the goal value θ^* in finite time and switch to a controller that moves to the goal value of r^* ; $\psi(t) = \psi^*$ can then be obtained by a rotation after the goal position is obtained. This is a weaker condition than asymptotic stability in the sense of Lyapunov.

The controller will be based on switched system control theory. The task space is $\mathcal{A} \triangleq \{r, \theta, \psi | r \in [r_{\min}, r_{\max}], \theta \in (-\pi, \pi], \psi \in \mathbb{S}^1\} \subset SE(2)$. Given a goal pose $\mathbf{X}^* = [r^*, \theta^*, \psi^*]^T \in \mathcal{A}$, there are three switching surfaces given in polar coordinates:

$$\begin{aligned} \mathcal{S}1 &\triangleq \{r, \theta, \psi\} \text{ s.t. } r = r_{\max} \\ \mathcal{S}2 &\triangleq \{r, \theta, \psi\} \text{ s.t. } r = r_{\min} \\ \mathcal{S}3 &\triangleq \{r, \theta, \psi\} \text{ s.t. } \theta = \theta^*. \end{aligned}$$

Without loss of generality, we can assume $\theta^* = 0$. These surfaces are illustrated in Fig. 3. The system has initial pose $\mathbf{X}(0) = [r(0), \theta(0), \psi(0)]^T \in \mathcal{A}$. We present a set of switching control laws for that the case that $\theta(0) > \theta^*$, i.e. the robot must move clockwise about the annulus.

The controller begins following the flow of the vector field described by

$$f_0 = \left[\cos(\tilde{\phi})\tilde{v}, -\frac{1}{r} \sin(\tilde{\phi})\tilde{v}, -\frac{1}{r} \sin(\tilde{\phi})\tilde{v} \right]^T \quad (10)$$

where $\tilde{v} > 0$ is a constant velocity input. The state variables $r(t)$ increases and $\theta(t)$ decreases. If the state contacts surface

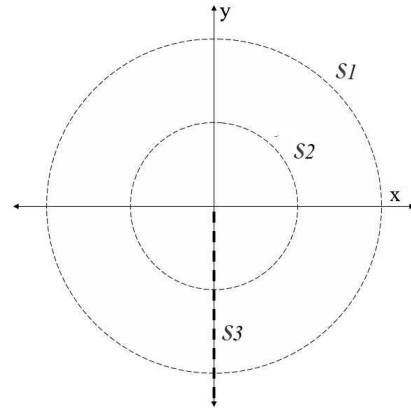


Fig. 3. Switching Surfaces for the Kinematic Unicycle Controller

$\mathcal{S}1$, the controller switches to follow the vector field

$$f_{s1} = \left[-\cos(-\tilde{\phi})\tilde{v}, \frac{1}{r} \sin(-\tilde{\phi})\tilde{v}, \frac{1}{r} \sin(-\tilde{\phi})\tilde{v} \right]^T \quad (11)$$

which decreases $r(t)$ and $\theta(t)$. If the state contacts surface $\mathcal{S}2$, the controller switches to follow the vector field

$$f_{s2} = f_0. \quad (12)$$

If the state contacts the surface $\mathcal{S}3$, the controller switches to follow the vector field

$$\begin{aligned} f_{s3} &= \left[\cos(0)\lambda(r(t) - r^*), -\frac{1}{r} \sin(0)\tilde{v}, -\frac{1}{r} \sin(0)\tilde{v} \right]^T \\ &= [\lambda(r(t) - r^*), 0, 0]^T \end{aligned} \quad (13)$$

where λ is a positive scalar gain. While not technically a T-curve (ϕ is not saturated), we will refer to the trajectory resulting from f_{s3} as a third available curve. Additionally, note that f_{s3} is in the span of f_{s1} and f_{s2} .

A set of control laws for $\theta(0) < \theta^*$ follows a similar development. The sets of laws for $\theta(0) > \theta^*$ and $\theta(0) < \theta^*$ together provide a switched system controller to regulate the state.

Theorem: Given initial pose $\mathbf{X}(0)$ and goal pose \mathbf{X}^* , the switched system controller is bounded and regulates the position such that

$$\lim_{t \rightarrow \infty} \mathbf{X}(t) = \mathbf{X}^* \quad (14)$$

Proof: First we prove that the state is bounded. The variable θ remains in $(-\pi, \pi]$ since the switching laws allow the robot to move CCW or CW to the goal. From equation (1), θ bounded $\Rightarrow \psi$ bounded. Thus, to prove that the state is bounded, it suffices to prove that \mathbf{X} is always in the annulus.

Hespanha showed that a region is invariant to a hybrid switched system control if at each point \mathbf{X} on the switching surfaces, the vector field $\dot{\mathbf{X}}$ at that point points toward the interior of the set [9].

For $\mathbf{X} \in \mathcal{S}1$, $\dot{\mathbf{X}} = f_{s1}$. From any point on $\mathcal{S}1$, the vector field points to the interior of the annulus if $|\tilde{v}| < r_{\max} - r_{\min}$ and if the T-curve is anything less than tangent to the circle.

This is true if $\tilde{\phi} < 90^\circ$, which is not feasible for a standard camera. A similar analysis holds for S_2 . For the surface $S_3 \subset \mathcal{A}$, $\dot{\mathbf{X}} = [\lambda(r(t) - r^*), 0, 0]^T$ points toward the interior of the annulus. Therefore, if \tilde{v} is sufficiently small the state never leaves the annulus, and the state is bounded.

Define the error signals

$$e_\theta(t) = \theta(t) - \theta^* \quad (15)$$

$$e_r(t) = r(t) - r^*. \quad (16)$$

We define a Lyapunov-like function

$$V_\theta = \frac{1}{2} e_\theta^2. \quad (17)$$

It is easy to see that $V_\theta > 0, \forall e_\theta \neq 0$.

When following vector field f_{s1} , combining (11) and (17) gives

$$\begin{aligned} \dot{V}_\theta &= e_\theta \dot{\theta} \\ &= e_\theta \frac{\tilde{v}}{r} \sin(-\tilde{\phi}) < 0. \end{aligned} \quad (18)$$

where $r(t)$ is bounded from below and above. Similarly, when following vector field f_{s2} ,

$$\begin{aligned} \dot{V}_\theta &= e_\theta \dot{\theta} \\ &= e_\theta \frac{-\tilde{v}}{r} \sin(\tilde{\phi}) < 0. \end{aligned} \quad (19)$$

Thus \dot{V}_θ is strictly decreasing along both vector fields f_{s1} and f_{s2} , and $\theta \rightarrow \theta^*$ in finite time.

When the $\theta(t) = \theta^*$, the state is on the surface S_3 and the system switches to follow f_{s3} . Define a new Lyapunov-like function

$$V = \frac{1}{2} (e_\theta^2 + e_r^2). \quad (20)$$

While following the flow of f_{s3} we have

$$\dot{\theta} = 0 \quad (21)$$

$$\dot{r} = \frac{\tilde{v}}{r} \sin(-\tilde{\phi}). \quad (22)$$

Equations (20)- (22) give

$$\dot{V} = e_r \frac{\tilde{v}}{r} \sin(-\tilde{\phi}) < 0 \quad (23)$$

Thus $\theta(t) = \theta^*$ and $r(t) \rightarrow r^*$ along the vector field f_{s3} , and the system is regulated to the goal position. At this point, ψ can be regulated by following the vector field f_3 given in (9) to the desired orientation.

V. VISION-BASED IMPLEMENTATION

The controller discussed in Sections II-IV assumes a landmark of a single point, that the distance to the origin is known at all time, and the ability to instantly switch between T-curves. In this Section we detail a controller for kinematic unicycle robots that uses a camera as the only input sensor. This controller will approximate the T-curves of the ideal controller while. While we do not prove the stability of this implemented controller, simulation and experimental results indicate it is capable of regulating the vehicle to a goal pose in the annulus.

By definition, a T-curve is being followed if the viewed landmark is kept on the edge of the field of view while the robot drives, i.e. $\phi \in \{-\tilde{\phi}, \tilde{\phi}\}$. An additional curve is available for driving on a radial line if $\phi = 0$. A real robot cannot switch instantaneously between the vector fields f_{s1} , f_{s2} , and f_{s3} since it cannot instantly obtain arbitrary values of ϕ . We must introduce modes of control that rotate the robot between the key values of $\phi \in \{-\tilde{\phi}, 0, \tilde{\phi}\}$. Noting that $\dot{\phi} = \dot{\psi}$, a control signal of the form (9) will rotate the robot to obtain the desired value of ϕ .

Assume, without loss of generality, that a visible landmark is located at the origin of the task space $SE(2)$. Given the goal pose \mathbf{X}^* and current pose $\mathbf{X}(t)$, it is necessary to define an annulus $\mathcal{A} \subset SE(2)$ such that $\mathbf{X}^*, \mathbf{X}(t) \in \mathcal{A}$. We use the goal radius r^* for r_{\min} . Choosing $r_{\min} = r^*$ insures that \mathbf{X}^* is in front of the robot when the robot is on the radial line $\theta(t) = \theta^*$. The choice of r_{\max} is somewhat arbitrary, but a multiple of r_{\min} is effective. In the results that follow we have used $r_{\max} = 2r^*$.

For the case that $\theta(0) \in [\theta^*, \pi]$ the robot should move clockwise around the annulus. A sequence of motions that will approximate T-curves to move clockwise from an initial pose in the annulus $\mathbf{X}(0)$ to the goal pose \mathbf{X}^* is outlined as follows:

- 1) Increase ψ until the landmark is on the extreme left edge of the image.
- 2) When $\phi = \tilde{\phi}$, drive backward and steer such that the image of the point remains on the left edge.
- 3) When $r = r_{\max}$ at the outside edge of the annulus, decrease ψ to place the landmark on the right edge of the image.
- 4) When $\phi = -\tilde{\phi}$, drive forward and steer such the point remains on the right edge of the image.
- 5) When robot is on the radial line described by $\theta = \theta^*$, rotate such that $\phi = 0$ and drive toward r^* .

A similar sequence is used for the case that $\theta(0) \in (-\pi, \theta^*]$, to move counterclockwise around the annulus.

We will henceforth refer to these as the five modes of operation. Modes 1 and 3 rotate the robot, allowing the choice of T-curves defined by $\phi = -\tilde{\phi}$ or $\phi = \tilde{\phi}$, and the third curve where $\phi = 0$. Modes 2 and 4 drive the robot along a T-curve by applying linear velocity while maintaining the constraint on saturating ϕ . Mode 5 first rotates until $\phi = 0$ and regulates the remaining radial error.

The minimum and maximum radii of the annulus describe two switching surfaces. When the robot is in mode 2 and crosses r_{\max} the system switches to mode 3. When the robot is in mode 4 and crosses r_{\min} the system switches to mode 1. The radial line $\theta = \theta^*$ defines a third switching surface. When this line is contacted under modes 2 or 4, we switch to mode 5. With $r_{\min} = r^*$, \mathbf{X}^* is in front of the robot when the robot is on the radial line $\theta(t) = \theta^*$.

It typically is not feasible to consider a point for a landmark, since vision-based control methods require three or more points [10], [11], [12]. If we now consider a collection of points centered at the origin, to approximate a T-curve the system must keep the rightmost point on the right edge of

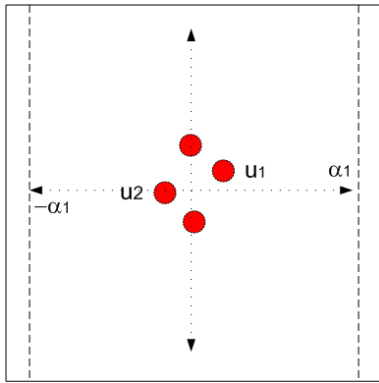


Fig. 4. Example Image

the image or the leftmost point on the left edge of the image. This effectively reduces ϕ and makes it dependent on r as the image of the landmark will be larger when r is small and less rotation will be feasible without points leaving the image. The vehicle trajectories will stray from true T-curves for large landmark objects and small r_{\min} .

We define several feedback control laws to accomplish the five modes of operation described at the beginning of this section. Defining the robot state space as in equation (4), with inputs v and ω , we use vision data and the current depth $r(t)$ in feedback loops. Given a collection of image points, define the rightmost point as $\mathbf{u}_1 = [u_1, v_1]^T$ and the leftmost point as $\mathbf{u}_2 = [u_2, v_2]^T$ in pixel coordinates. It is desired to keep the points near the edge of the image, thus define widths α , $-\alpha$ near the edges. This is illustrated in Fig. 4.

Feedback control laws

$$\omega = \lambda_\omega(-\alpha - u_1) \quad (24)$$

$$\omega = \lambda_\omega(\alpha - u_2), \quad (25)$$

where and λ_ω is a positive scalar gain, will rotate the robot such that the landmark is regulated to the right or left the edge of the image, respectively. Control laws

$$v = \lambda_v(2r^* - r(t)) \quad (26)$$

$$v = \lambda_v(r^* - r(t)), \quad (27)$$

where λ_v is a positive scalar gain will drive the robot toward the outer and inner radius of the annulus, respectively.

Given these basic feedback control laws, a series of proportional control laws to perform the modes of operation are presented. A similar set of controls is defined for moving counterclockwise about the annulus.

1) Increase ψ :

$$v = 0$$

$$\omega = \lambda_\omega(-\alpha - u_1) + \varepsilon_\omega$$

2) When $\phi = \tilde{\phi}$, drive back and steer:

$$v = \lambda_v(2r^* - r(t)) - \varepsilon_v$$

$$\omega = \lambda_\omega(-\alpha - u_1)$$

3) When $r = r_{\max}$, decrease ψ :

$$v = 0$$

$$\omega = \lambda_\omega(\alpha - u_2) - \varepsilon_\omega$$

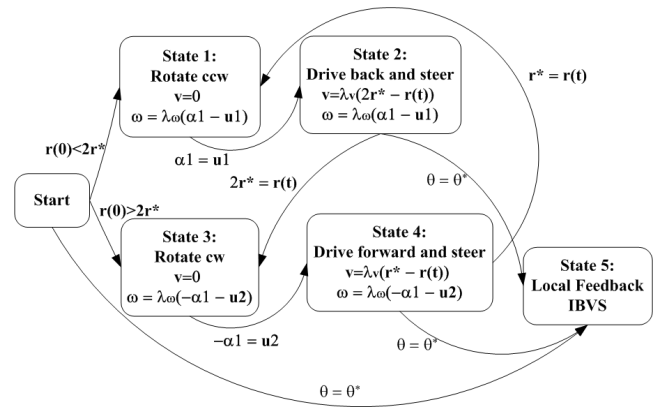


Fig. 5. Finite State Diagram for Moving Counter Clockwise Around the Annulus

4) When $\phi = -\tilde{\phi}$, drive forward and steer:

$$v = \lambda_v(r^* - r(t)) + \varepsilon_v$$

$$\omega = \lambda_\omega(\alpha - u_2)$$

5) When $\theta = \theta^*$, rotate s.t. $\phi = 0$

$$\omega = \lambda_\omega((\theta + \pi) - \psi(t)) + \text{sgn}(\theta + \pi - \psi(t))\varepsilon_\omega$$

then drive forward:

$$v = \lambda_v(2r^* - r(t))$$

$$\omega = 0$$

In these feedback control laws, and ε_ω and ε_v are small, positive constant scalars to insure the state reaches the switching surfaces in finite time.

It is necessary to determine in which state the system begins. After that, switches occur when crossing a switching surface. If $r(0) < r_{\max}$, begin at step 1 to move backwards. If $r(0) > r_{\max}$ begin at step 3. Note that this also allows for cases where $\mathbf{X}(0)$ is not in the annulus. These steps are illustrated in a finite state diagram Fig. 5.

A final limitation of the vision-based implementation concerns the ability to estimate the pose given the visible landmark. It is likely that the points on the landmark are visible only within a subset of the annulus. A nonplanar landmark can occlude parts of itself. Even given a planar landmark, the points are likely visible only from half the annulus. While most any pose reconstruction method could be used to get the state $\mathbf{X}(t)$ (e.g. [12], [13], [14]), we use the well known Euclidean Homography matrix between images of planar points [14], [15].

There are numerous issues that can influence performance. We will discuss them briefly but leave them to future work. Signal noise, robustness of the robot model and camera and robot calibration clearly can have adverse affects. Also, outside of an ideal environment, it is possible for the robot to leave the line $\theta = \theta^*$ when in mode 5. This would necessitate a return to modes 1 or 3, which could result in chattering effects. A better solution would entail using a more advanced controller for mode 5 to reject disturbances of θ .

VI. EXPERIMENTAL RESULTS

Simulations were performed using the implementation of Section V. The landmark is a square of coplanar points.

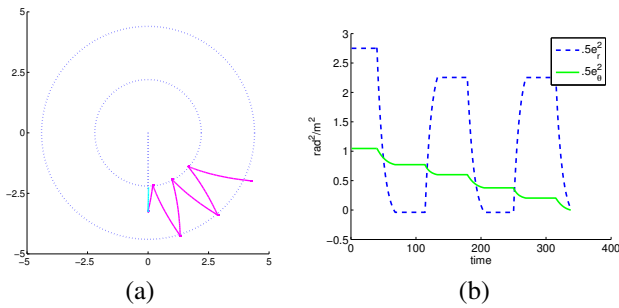


Fig. 6. Simulation Results

We assume an image of the landmark taken at \mathbf{X}^* and knowledge of the feature point at the goal are known. With this information we use the homography between images of planar points to estimate the robot's coordinates $\mathbf{X}(t)$. See the Appendix for details on this pose reconstruction technique.

The robot starts from position $[r, \theta, \psi]^T = [2.75, \pi/3, 5\pi/6]^T$, and the goal position is $[-1.2, 0, 0]^T$. Fig. 6(a) shows the path taken by the robot along with the switching surfaces; Fig. 6(b) shows the values of $e_\theta = \theta(t) - \theta^*$ and $e_r = r(t) - r^*$ over time. The distance error, e_r is bounded and periodic, while values of e_θ tends to zero as time increases. The robot eventually reaches the radial line where $e_\theta = 0$. Then the remaining error in $r(t)$ is regulated to zero. These results agree with what is expected from the proof of stability for the ideal system in Section IV.

We have implemented the control scheme with a robot for real experiments. At the time of publication, the true robot position values were unavailable, and position estimates from encoder values was too noisy to be insightful. Video of the system is informative, and an example can be found in the video proceedings and at http://www-cvr.ai.uiuc.edu/~ngans/segbot_video.wmv. The robot uses a Texas Instruments TMS320 DSP for all signal processing and motor control. An OmniVision OV6620 Color CMOS camera provides vision data. No other environmental sensors were used. The landmark is a square of four LED's. The controller works well, especially considering the coarse camera resolution and the low processor bandwidth.

VII. CONCLUSION

Control of nonholonomic systems, such as wheeled vehicles, is a difficult problem, especially when sensor limitations are taken into account. Bhattacharya et al. [6] developed control scheme for a wheeled robot which can keep an landmark in the field of a mounted camera. We have also demonstrated the controllability and stability of the control scheme in that the robot can move to any point in an annulus surrounding a visible landmark. We have further developed the scheme for a vision-based implementation of this control scheme using a system of feedback controllers. Simulations of the implemented controller are provided, along with video of experiments using a mobile robot.

Future work will focus on establishing the stability and controllability of the vision-based implementation of the motion scheme. Additionally, alternative implementations could be devised, including ones that do not require a priori knowledge of the goal pose, but rely only on data directly available from image data.

VIII. ACKNOWLEDGMENTS

We would like to thank Mark Spong and Dan Block of the University of Illinois Control Systems Instructional Laboratory [16] for the use of the Segbot. This material is based in part upon work supported by the National Science Foundation under Award Nos. CCR-0085917 and IIS-0083275.

REFERENCES

- [1] J. Laumond and J. Risler, "Nonholonomic systems: controllability and complexity," 1996.
- [2] R. Pissard-Gibollet and P. Rives, "Applying visual servoing techniques to control a mobile hand-eye system," in *Proc. of the International Conference on Robotics and Automation*, vol. 1, pp. 166 – 171, 1995.
- [3] Y. Ma, J. Kosecka, and S. Sastry, "Vision guided navigation for a nonholonomic mobile robot," *IEEE Transactions on Robotics and Automation*, vol. 15, no. 3, pp. 521–537, 1999.
- [4] Y. Fang, D. Dawson, W. Dixon, and M. de Queiroz, "Homography-based visual servoing of wheeled mobile robots," in *2002, Proc. IEEE Conf. on Decision and Control*, pp. 2866 – 2871, 2002.
- [5] G. Kantor and A. Rizzi, "Sequential composition for control of underactuated systems," tech. rep., Robotics Institute, Carnegie Mellon University, Nov. 2003. www.msl.rpi.edu/publications/pdfs/kantor_george_a.2003.1.pdf.
- [6] S. Bhattacharya, R. Murrieta-Cid, and S. Hutchinson, "Path planning for a differential drive robot: Minimal length paths—a geometric approach," in *Proc. Int. Conf. Intelligent Robots and Systems*, 2004.
- [7] S. M. LaValle, *Planning Algorithms*. [Online], 2004. Available at <http://msl.cs.uiuc.edu/planning/>.
- [8] H. Choset, K. M. Lynch, S. Hutchinson, G. K. W. Burgard, L. E. Kavraki, and S. Thrun, *Principles of Robot Motion: Theory, Algorithms, and Implementations*. Boston: MIT Press, 2005.
- [9] J. Hespanha, "Stabilization of nonholonomic integrators via logic-based switching," in *Proc. of the 13th World Congress of Int. Federation of Automat. Contr.*, June 1996.
- [10] O. Faugeras and F. Lustman, "Motion and structure from motion in a piecewise planar environment," 1988.
- [11] Z. Zhang and A. Hanson, "3d reconstruction based on homography mapping," in *Proc. ARPA Image Understanding Workshop, Palm Springs, CA*, 1996.
- [12] D. DeMenthon and L. S. Davis, "Model-based object pose in 25 lines of code," in *European Conference on Computer Vision*, pp. 335–343, 1992.
- [13] L. Quan and Z.-D. Lan, "Linear n-point camera pose determination," *IEEE Transactions on Pattern Analysis and Machine Intelligence*, vol. 21, no. 8, pp. 774–780, 1999.
- [14] Y. Ma, S. Soatto, J. Koseck, and S. Sastry, *An Invitation to 3-D Vision*. Springer, 2004.
- [15] O. Faugeras, *Three-Dimensional Computer Vision*. Cambridge, MA: MIT Press, 1993.
- [16] A. Alleyne, D. Block, S. M. W.R., Perkins, and M. Spong, "An interdisciplinary, interdepartmental control systems laboratory," 2005.